Electronic Supporting Information

Crystallographic (C), DFT and Electrochemical (E) data

Group-6 Metal Complexes as Electrocatalysts of CO_2 Reduction: Strong Substituent Control of the Reduction Path of [Mo(η^3-allyl)(CO)$_2$(*x*,*x′*-dimethyl-2,2′-bipyridine)(NCS)] (*x* = 4-6)

James O. Taylor,[1] Florentine L. P. Veenstra,[1,2] Ann M. Chippindale,[1] Maria José Calhorda,[3] František Hartl[1,*]

[1]Department of Chemistry, University of Reading, Reading, RG6 6AD, United Kingdom.

[2]Institute for Chemical and Bioengineering, Department of Chemistry and Applied Biosciences, ETH Hönggerberg, Vladimir-Prelog-Weg 1, 8093 Zurich, Switzerland

[3] Centro de Química e Bioquímica and BioISI - Biosystems & Integrative Sciences Institute, Departamento de Química e Bioquímica, Faculdade de Ciências, Universidade de Lisboa, 1749-016 Lisboa, Portugal

Corresponding Author

E-mail: f.hartl@reading.ac.uk

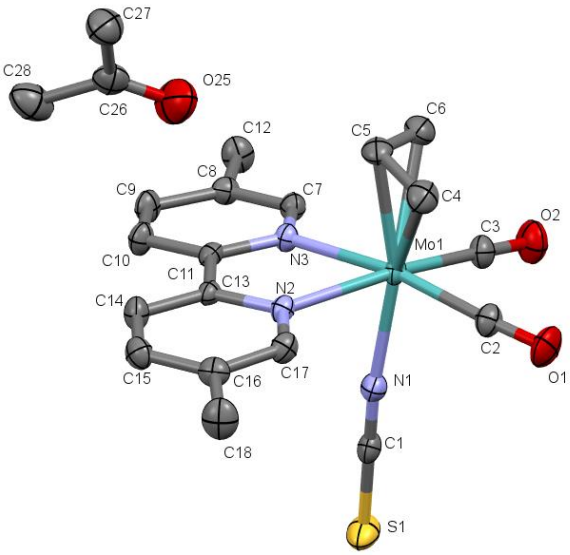

Figure C-S1. An ORTEP view (50% thermal probability) of the molecular structure of [Mo(η^3-allyl)$(CO)_2$(5,5′-dmbipy)(NCS)] (**2**) determined by single-crystal X-ray analysis. Hydrogen atoms have been omitted for clarity. The crystal structure also contains one molecule of the solvent acetone.

Table C-S1. Crystallographic data for **1**-**3**.

Complex	**3** with 6,6′-dmbipy	**2** with 5,5′-dmbipy	**1** with 4,4′-dmbipy
Formula	C18H17MoN3O2S [+ solvent]	C18H13MoN3O2S, C3H6O	C18H17Mo1N3O2S1
M_r	435.35 [a]	489.39	435.36
Crystal system	orthorhombic	monoclinic	orthorhombic
Space group	*Pbca*	$P2_1/c$	*Pnam*
Z	8	4	4
a/Å	15.0540(5)	10.3391(4)	15.2602(5)
b/Å	14.6980(4)	19.3368(5)	8.3477(3)
c/Å	17.9270(5)	11.5027(4)	14.2157(4)
α/°	90	90	90
β/°	90	105.951(3)	90
γ/°	90	90	90
V/Å^3	3966.6(2)	2211.13(13)	1810.89(11)
ρ_{calc}/g cm^{-1}	1.458 [a]	1.470	1.597
Crystal habit	Red plate	Red plate	Red block
Crystal dimensions /mm	0.03×0.06×0.07	0.036×0.053×0.100	0.050×0.055×0.060
Radiation	Mo Kα	Mo Kα	Mo Kα
T/K	150	150	150
μ/mm^{-1}	0.781 [a]	0.713	0.856
R(F), R_w(F)	0.0463, 0.0374	0.0398, 0.0156	0.0512, 0.0313
CCDC Code	1862264	1862263	1862262

[a] Excludes solvent.

Table C-S2. Selected bond lengths (Å) and angles (°) for **1**-**3**.

Complex	**3** with 6,6′-dmbipy	**2** with 5,5′-dmbipy	**1** with 4,4′-dmbipy
Mo(1)–N(2)	2.296(2)	2.254(1)	2.240(2)
Mo(1)–N(3)	2.289(2)	2.237(1)	2.240(2)
Mo(1)–C(4)	2.341(3)	2.325(2)	2.331(2)
Mo(1)–C(5)	2.232(3)	2.220(2)	2.214(3)
Mo(1)–C(6)	2.338(3)	2.339(2)	2.331(2)
Mo(1)–C(2)	1.949(3)	1.978(2)	1.958(2)
Mo(1)–C(3)	1.953(3)	1.951(2)	1.958(2)
C(2)–O(1)	1.166(4)	1.155(2)	1.161(3)
C(3)–O(2)	1.156(3)	1.157(2)	1.161(1)
Mo(1)–N(1)	2.135(2)	2.149(1)	2.135(2)
N(1)–C(1)	1.162(3)	1.160(2)	1.186(2)
C(1)–S(1)	1.626(3)	1.626(2)	1.614(1)
N(2)–Mo(1)–N(3)	72.80(8)	72.95(5)	72.90(8)
C(2)–Mo(1)–C(3)	76.10(12)	80.67(7)	82.59(13)

Table DFT-S1. DFT-calculated energies (kcal mol^{-1}) for **1**, **2**, and **3** (= **X**), their radical anions [**X**]$^{\bullet-}$ and derived 5-coordinate radicals [**X**-R], 5-coordinate anions ([**X**-A]$^{-}$ (obtained by the loss of thiocyanate), 6-coordinate anions [**X**-PrCN]$^{-}$ and [**X**-CO_2]$^{-}$, and dimers [**X**-D]. (For the molecular structures see Scheme 1 and the DFT section in the main text.)

Complex	**1**	**2**	**3**	Others
X eq	-6330.74	-6329.63	-6323.25	
X ax	-6330.07	-6328.77	-6317.80	
[**X**]$^{\bullet-}$ eq	-6393.97	-6391.81	-6387.50	
[**X**]$^{\bullet-}$ ax	-6394.79	-6392.86	-6381.65	
[X-R] SP	-5823.55	-5822.38	-5814.17	
[**X**-R] TBP	-5823.98	-5822.82	-5809.34	
[**X**-A]$^{-}$ diamag.	-5895.45	-5895.03	-5883.54	
[**X**-A]$^{-}$ paramag.	-5878.54	-5875.86	-5871.77	
[**X**-PrCN]$^{-}$ eq, diamag.	-7471.01	-7431.32	-7467.35	
[**X**-D]	-11658.23	-11656.03	-	
[**X**-CO_2]$^{-}$ eq	-6435.03			
[**X**-CO_2]$^{-}$ ax	-6427.82			
x,x'-dmbipy	-3836.23			
[**X**-(*x,x'*-dmbipy)]				-2453.28
PrCN				-1593.63
CO_2				-531.74
SCN^{-}				-526.59

Table DFT-S2. DFT-calculated relative energies (kcal mol^{-1}) for **1**, **2**, and **3** (= **X**), their radical anions [**X**]$^{\bullet-}$ and derived 5-coordinate radicals [**X**-R,], 5-coordinate anions ([**X**-A]$^{-}$ (obtained by the loss of thiocyanate), 6-coordinate anions [**X**-PrCN]$^{-}$, and dimers [**X**-D].

Complex	**1**	**2**	**3**
X eq	0	1.11	7.49
X ax	0.23	1.97	12.94
Δ*E*	0.23	0.86	5.45
[**X**]$^{\bullet-}$ eq	0.82	2.98	7.29
[**X**]$^{\bullet-}$ ax	0	1.93	13.14
Δ*E*	0.82	1.05	-5.95
[**X**-R] SP	0.43	1.60	9.81
[**X**-R] TBP	0	1.16	14.64
Δ*E*	0.43	0.44	-4.83
[**X**-A]$^{-}$ TBP	0	0.42	11.91
[**X**-PrCN]$^{-}$	0	-0.31	3.66
[**X**-D]	0	2.20	
ΔE_1 [a]	10.27	10.39	
ΔE_2 [b]	-41.37	-42.04	

[a] $\Delta E_1 = E$([**X**-D]) – 2 E([**X**-R]). [b] $\Delta E_2 = E$([**X**-D]) – E([**X**-A])-[E([**X**] eq)-E(SCN^{-})].

Table DFT-S3. Relevant DFT-calculated distances (Å) in **1**, **2**, and **3** (= **X**), as well as their radical anions [**X**]$^{\bullet-}$ and derived 5-coordinate radicals [**X**-R] and reduced 5-coordinate anions [**X**-A]$^{-}$ (obtained by the loss of thiocyanate).

Complex		**X**		[**X**]$^{\bullet-}$		[**X**-R]		[**X**-A]$^{-}$
	Exp (eq)	**equat**	axial	**equat**	axial	SP	**TBP**	from ax
1								
Mo–C1	2.331	**2.362**	2.369	**2.356**	2.382	2.327	**2.349**	2.41
Mo–C2	2.214	**2.252**	2.225	**2.241**	2.237	2.198	**2.236**	2.268
Mo–C3	2.331	**2.365**	2.329	**2.359**	2.348	2.328	**2.387**	2.402
Mo–C(O)	1.958	**1.965**	1.957	**1.966**	1.953	1.956	**1.943**	1.931
Mo–C(O)	1.958	**1.966**	1.966	**1.966**	1.956	1.956	**1.936**	1.948
Mo–N (trans CO)	2.24	**2.272**	2.307	**1.396**	2.29	2.188	**2.234**	2.207
Mo–N	2.24	**2.274**	2.226	**1.396**	2.181	2.189	**2.161**	2.14
C–C (inter–ring bipy)	1.489	**1.476**	1.473	**1.428**	1.428	1.446	**1.449**	1.432
Mo–N(CS)	2.134	**2.117**	2.177	**2.14**	2.218	-	-	-
N–C	1.186	**1.186**	1.185	**1.183**	1.183	-	-	-
C–S	1.614	**1.628**	1.632	**1.636**	1.641	-	-	-
2								
Mo–C1	2.339	**2.363**	2.368	**2.355**	2.385	2.327	**2.352**	2.408
Mo–C2	2.22	**2.254**	2.225	**2.241**	2.238	2.199	**2.235**	2.268
Mo–C3	2.325	**2.367**	2.328	**2.358**	2.352	2.328	**2.384**	2.401
Mo–C(O)	1.951	**1.966**	1.957	**1.966**	1.952	1.955	**1.942**	1.931
Mo–C(O)	1.978	**1.966**	1.966	**1.966**	1.966	1.956	**1.937**	1.949
Mo–N (trans CO)	2.237	**2.273**	2.312	**2.244**	2.293	2.191	**2.24**	2.207
Mo–N	2.254	**2.276**	2.229	**2.246**	2.179	2.193	**2.163**	2.141
C–C (inter–ring bipy)	1.473	**1.471**	1.468	**1.43**	1.431	1.446	**1.449**	1.434
Mo–N(CS)	2.148	**2.116**	2.177	**2.143**	2.224	-	-	-
N–C	1.16	**1.186**	1.186	**1.183**	1.183	-	-	-
C–S	1.626	**1.628**	1.632	**1.637**	1.642	-	-	-
3								
Mo–C1	2.338	**2.37**	2.36	2.361	2.352	**2.325**	nc[a]	**2.326**
Mo–C2	2.232	**2.252**	2.239	2.244	2.238	**2.201**	nc	**2.211**
Mo–C3	2.341	**2.37**	2.347	2.363	2.344	**2.317**	nc	**2.328**
Mo–C(O)	1.953	**1.956**	1.945	1.957	1.948	**1.954**	nc	**1.961**
Mo–C(O)	1.949	**1.955**	1.963	1.956	1.957	**1.954**	nc	**1.961**
Mo–N (trans CO)	2.289	**2.333**	2.365	2.297	2.322	**2.234**	nc	**2.185**
Mo–N	2.296	**2.331**	2.273	2.293	2.25	**2.235**	nc	**2.187**
C–C (inter–ring bipy)	1.483	**1.482**	1.478	1.433	1.428	**1.454**	nc	**1.421**
Mo–N(CS)	2.135	**2.112**	2.273	2.136	2.199	-	-	-
N–C	1.162	**1.186**	1.186	1.184	1.184	-	-	-
C–S	1.626	**1.627**	1.632	1.636	1.639	-	-	-

[a] Not converged.

Table DFT-S4. Energy decomposition for the interaction between the *x,x′*-dmbipy ligand and the {Mo(η^3-allyl)$(CO)_2$(NCS)} fragment in the equatorial isomer of **1-3** (energies in kcal mol^{-1}).

Complex	**1**	**2**	**3**
ΔE_{Pauli}	134.40	134.26	127.73
ΔE_{elec}	-120.49	-120.26	-112.02
ΔE_{oi}	-69.36	-69.28	-64.36
ΔE_{int}	-55.44	-55.28	-48.65
ΔE_{prep}	10.45	10.42	9.97
ΔE_{prep}	2.08	1.81	4.51
ΔE_{prep}	12.53	12.23	14.48
$\boldsymbol{\Delta E_{lig}}$	**-42.91**	**-43.05**	**-34.17**

In the EDA,[1] the interaction energy (ΔE_{int}) is considered as the sum of Pauli repulsion (ΔE_{Pauli}), electrostatic (ΔE_{elec}) and orbital interactions (ΔE_{oi}). ΔE_{Pauli} represents the repulsion between occupied orbitals of the fragments, ΔE_{elec} the electrostatic interaction between fragments, and ΔE_{oi} the 2-electron stabilizing interactions between occupied levels of one fragment and empty levels of the other. ΔE_{elec} is an attractive term and ΔE_{oi} is related to covalent bond formation. To calculate the bond energy (ΔE), another term must be considered, that is the reorganization or preparation energy (ΔE_{prep}). It corresponds to the difference between the energy of each fragment as it is in the complex and being allowed to relax to the lowest energy geometry.

References

1. a) Ziegler, T.; Rauk, A. *Inorg. Chem.* **1979**,*18*, 1755-1759. b) Ziegler, T.; Rauk, A. *Theor. Chim. Acta* **1977**, *46*, 1-10.

Table DFT-S5. DFT (ADF)-calculated frequencies of the symmetric and antisymmetric CO-stretching modes and the CN-stretching mode of thiocyanate (in cm^{-1}) in **1**-**3** (= **X**) and their reduction products (see Scheme 1).

Complex	**X**	[**X**]$^{\bullet-}$		[**X**-R]			[**X**-A]$^{-}$	[**X**-PrCN]$^{-}$	[**X**-D]
	Equatorial	Equatorial	Axial	SP	TBP	SP	TBP		
1									
ν_s(C≡O)	1882	1855	1841	1856	1834	-	1741	1797	1858,
ν_a(C≡O)	1800	1763	1750	1754	1746	-	1656	1705	1844
ν(N≡C)	2056	2070	2070	-	-	-	-	2229	1787, 1775 [a]
2									
ν_s(C≡O)	1883	1853	1839	1851	1834	-	1742	1781	1859,
ν_a(C≡O)	1801	1761	1748	1754	1746	-	1658	1687	1844
ν(N≡C)	2056	2072	2068	-	-	-	-	2313	1789, 1777 [a]
3									
ν_s(C≡O)	1881	1855	1852	1852	-	1803		1816	-
ν_a(C≡O)	1800	1764	1759	1760	-	1702		1715	-
ν(N≡C)	2054	2069	2068	-	-	-		2247	-

[a] Four calculated ν(CO) modes of the dimer.

Table DFT-S6. Calculated and experimental excitation energies (eV), composition (%) and oscillator strengths (OS).

No.	λ/nm	E/eV	Composition (%)	λ/nm (exp)	OS
			[Mo(η^3-allyl)(CO)$_2$(4,4'-dmbpy)(NCS)] (1)		
1	506	2.45	H→L+1 (97)	490 (THF)	0.029
2	452	2.75	H-3→L (97)		0.082
3	347	3.57	H-2→L+3 (70), H-2→L+2 (23)		0.204
4	313	3.96	H-5→L (63), H-4→L+1 (24)		0.476
5	300	4.13	H-4→L+1 (71), H-5→L (17)		0.301
			[Mo(η^3-allyl)(CO)$_2$(5,5'-dmbpy)(NCS)] (2)		
1	506	2.44	H→L+1(54), H→L+2 (43)	480 (THF)	0.022
2	444	2.79	H-3→L (97)		0.081
3	385	3.22	H-2→L+2 (42), H-2→L+1 (42), H-2→L+3 (15)		0.087
4	354	3.50	H-2→L+3 (82), H-2→L+1 (7)		0.228
5	329	3.77	H-4→L (30), H-3→L+3 (26), H→L+4 (19), H-5→L (13)		0.354
6	325	3.81	H→L+4 (77), H-4→L (14)		0.129
7	324	3.83	H-3→L+3 (71), H-4→L (12), H-5→L (7)		0.250
			[Mo(η^3-allyl)(CO)$_2$(6,6'-dmbpy)(NCS)] (3)		
1	471	2.63	H→L+2 (68), H→L+3 (31)	460 (THF)	0.005
2	456	2.72	H-3→L(98)		0.040
3	449	2.76	H→L+3 (67), H→L+2 (29)		0.014
4	355	3.49	H-2→L+2 (72), H-2→L+3(22)		0.328
5	339	3.65	H-3→L+2 (50), H-4→L (18), H-5→L (18), H-3→L+3 (10)		0.135
6	332	3.73	H-3→L+2 (48), H-4→L (21), H-5→L (17)		0.277

TDDFT calculations were performed to analyze the electronic absorption of the parent complexes, which reflects their bonding properties. Calculated complex **1** exhibits two major absorptions at 506 and 452 nm (Table DFT-S6, Supporting Information), in relatively good agreement with the experimental UV-vis spectra showing an asymmetric absorption band between 400-550 nm with a shallow absorption maximum at 470 nm. These visible optical excitations result from the HOMO-to-LUMO+1 and HOMO-3-to-LUMO transitions, respectively. The lowest-energy HOMO-to-LUMO+1 is essentially a (M-L)L′CT transition from occupied π*(Mo–NCS) to π*(4,4′-dmbipy) (see Figure 6 in the main text). Model complex **2** also exhibits two transitions at 506 nm (HOMO-to-LUMO+1, 54%, and HOMO-to-LUMO+2, 43%) and 444 nm (HOMO-3-to-LUMO), also close to the experimental λ_{max} value of 470 nm. Their nature is close to that described for **1**, involving excitation from π*(Mo–NCS) to π*(5,5′-dmbipy) but also to π*(Mo-allyl) (a small component). The MOs involved are shown in Figure DFT-S3 (Supporting Information). Complex **3** shows three electronic absorptions in the visible region, one at 471 nm (very weak) and two at 456 (HOMO-3-to-LUMO) and 449 nm (HOMO-to-LUMO+3, 67 %, HOMO-to-LUMO+2, 29%). Inspecting these orbitals (Figure DFT-S4, Supporting Information) points again to photoinduced charge transfer from π*(Mo–NCS) to π*(6,6′-dmbipy) and π*(Mo-allyl).

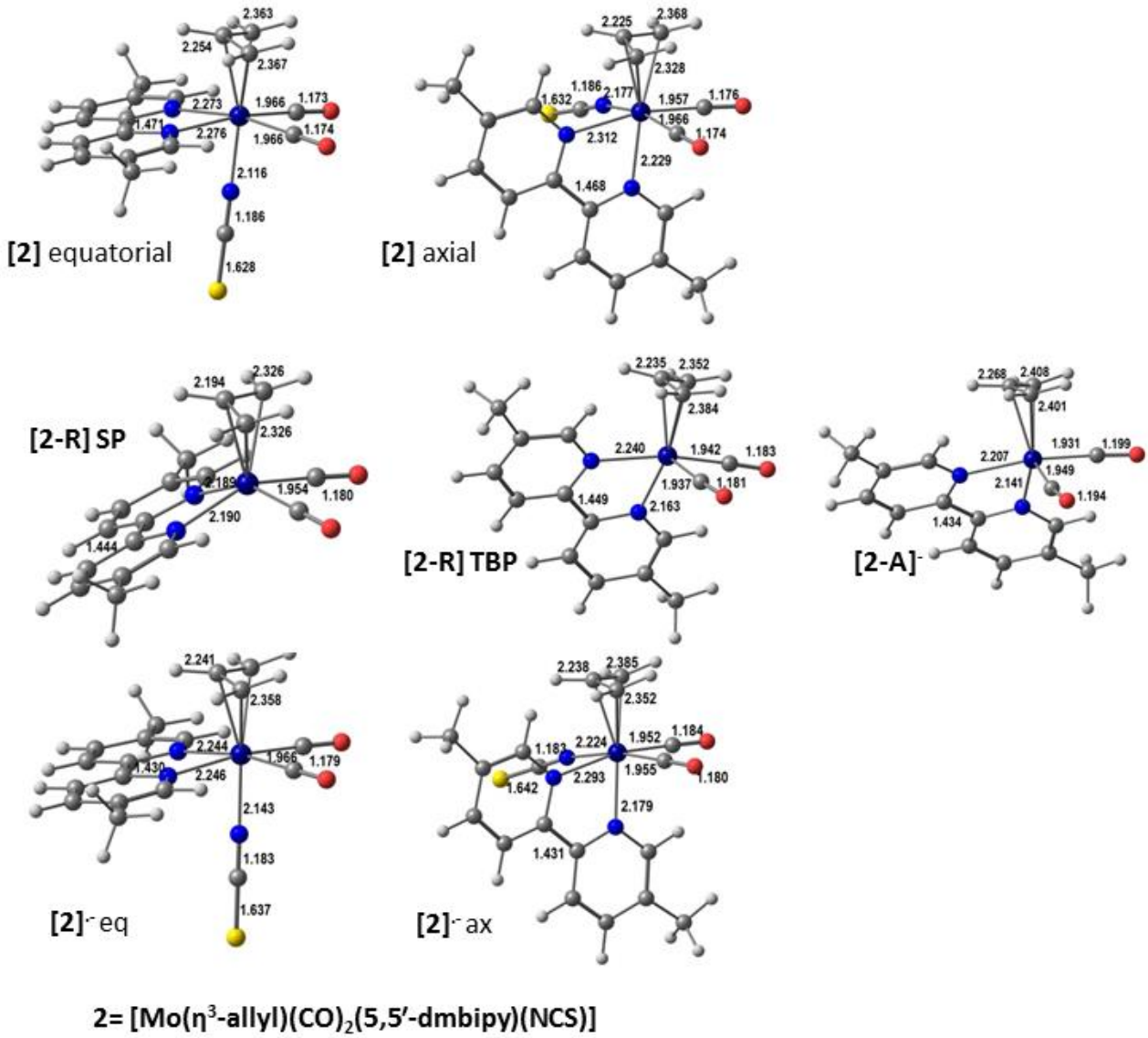

Figure DFT-S1. DFT-optimized structures of the parent complex [Mo(η^3-allyl)(CO)$_2$(5,5′-dmbipy)(NCS)] (**2**) (the equatorial isomer (top left), the axial isomer (top right), 1e$^-$ reduced radical anion [**2**]$^{\bullet-}$ (bottom left), 5-coordinate radical [**2**-R] (the SP isomer (center left), the TBP isomer (center right), and 2e$^-$ reduced 5-coordinate anion **[2**-A]$^-$ (bottom right), with the relevant bond lengths (Å).

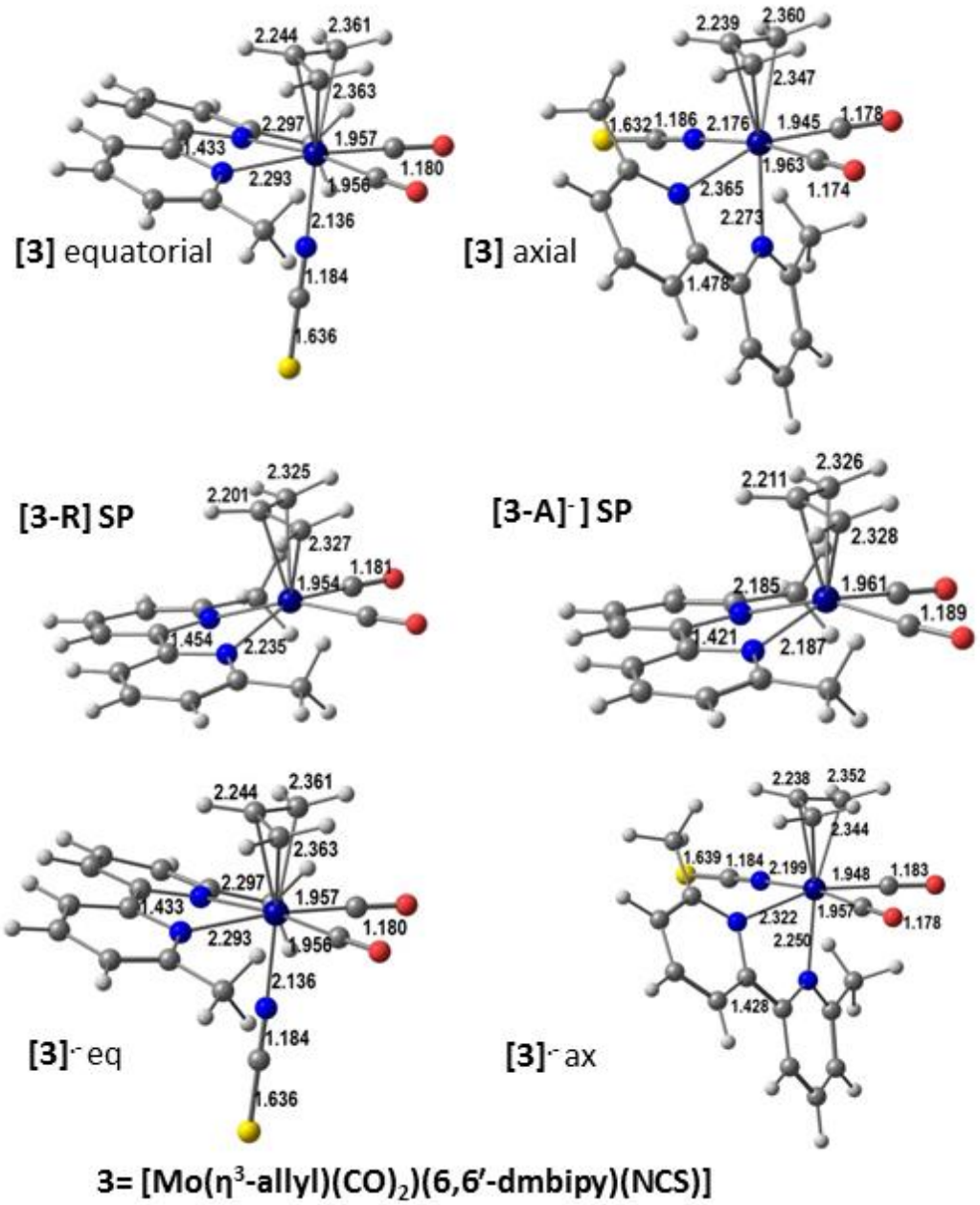

Figure DFT-S2. DFT-optimized structures of the parent complex [Mo(η^3-allyl)$(CO)_2$(6,6′-dmbipy)(NCS)] (**3**) (the equatorial isomer (top left), the axial isomer (top right), 1e$^-$ reduced radical anion [**3**]$^{\bullet-}$ (bottom left), 5-coordinate radical [**3**-R] (the SP isomer (center left), the TBP isomer (center right), and 2e$^-$ reduced 5-coordinate anion **[3**-A]$^-$ (bottom right), with the relevant bond lengths (Å).

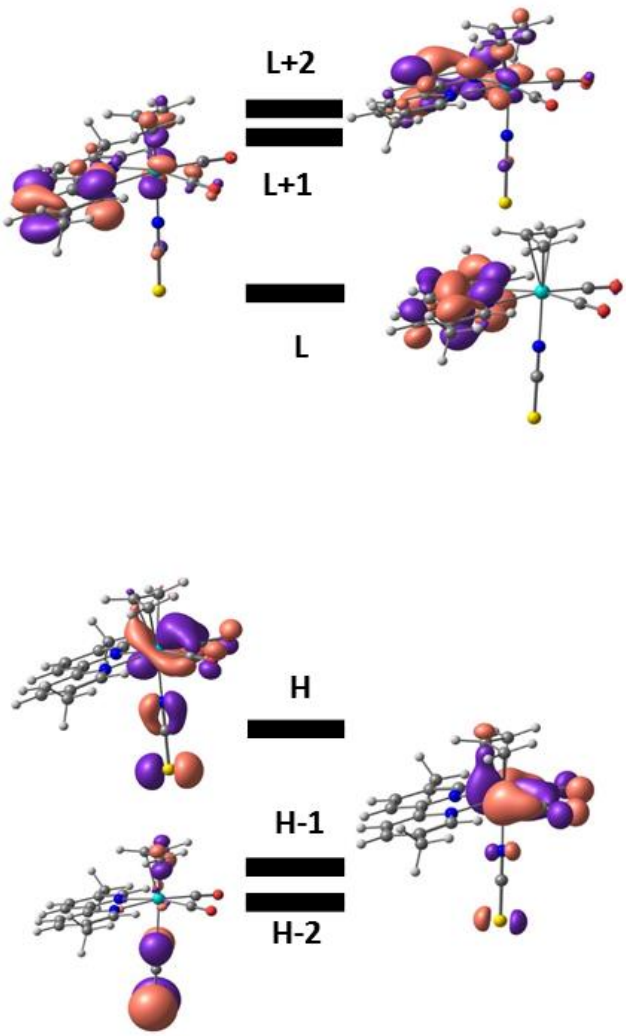

Figure DFT-S3. DFT-calculated frontier orbitals of the parent complex [Mo(η^3-allyl)$(CO)_2$(5,5′-dmbipy)(NCS)] (**2**). The HOMO-LUMO (H-L) gap is 1.616 eV.

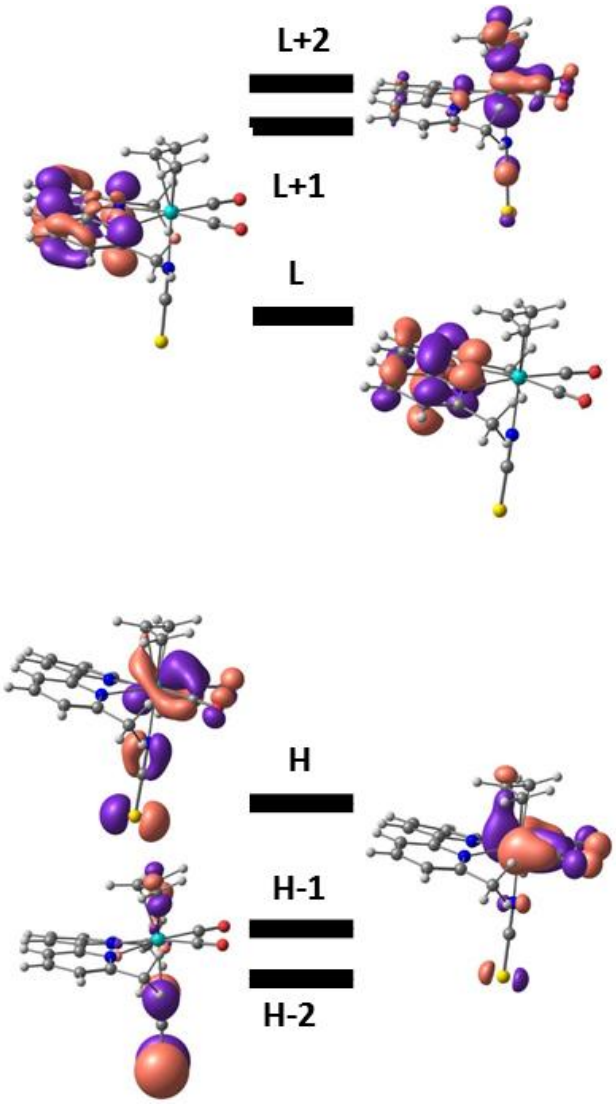

Figure DFT-S4. DFT-calculated frontier orbitals of the parent complex [Mo(η^3-allyl)$(CO)_2$(6,6′-dmbipy)(NCS)] (**3**). The HOMO-LUMO (H-L) gap is 1.592 eV.

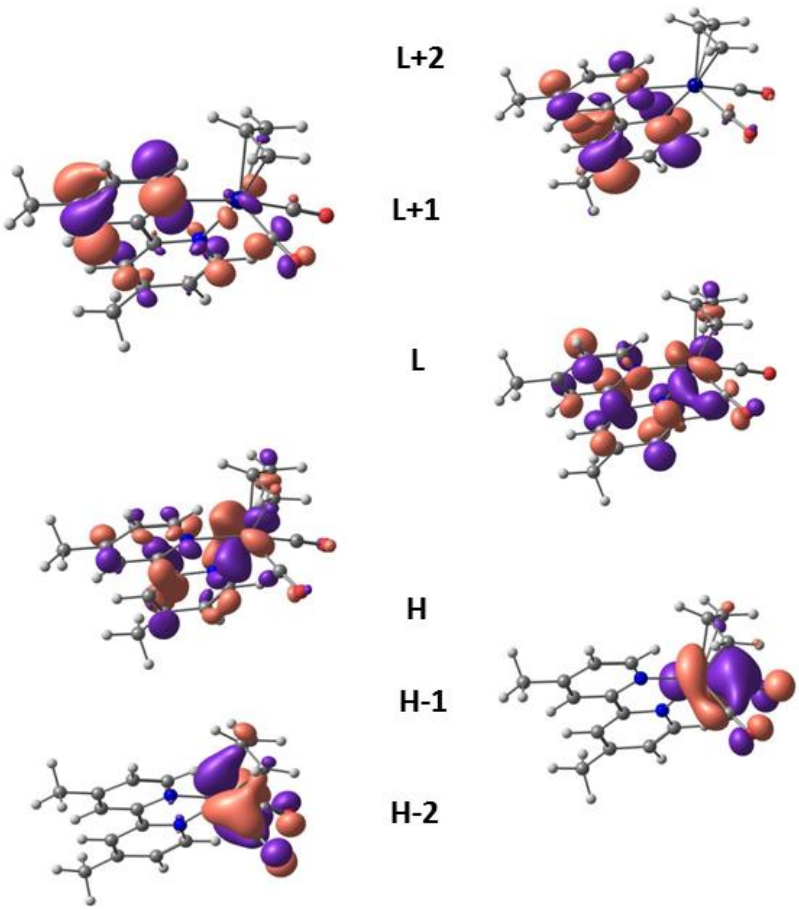

Figure DFT-S5. DFT-calculated α spin frontier orbitals of the 5-coordinate radical [Mo(η^3-allyl)$(CO)_2$(4,4′-dmbipy)], [**1**-R].

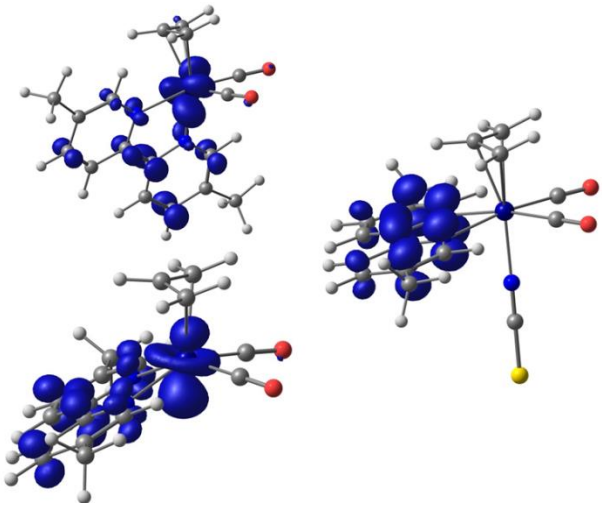

Figure DFT-S6. DFT-calculated spin densities in the 5-coordinate radical [Mo(η^3-allyl)$(CO)_2$(5,5′-dmbipy)], [**2**-R] (the TBP isomer (top left) and the SP isomer (bottom left)), and radical anion [**2**]$^{\bullet-}$ (right).

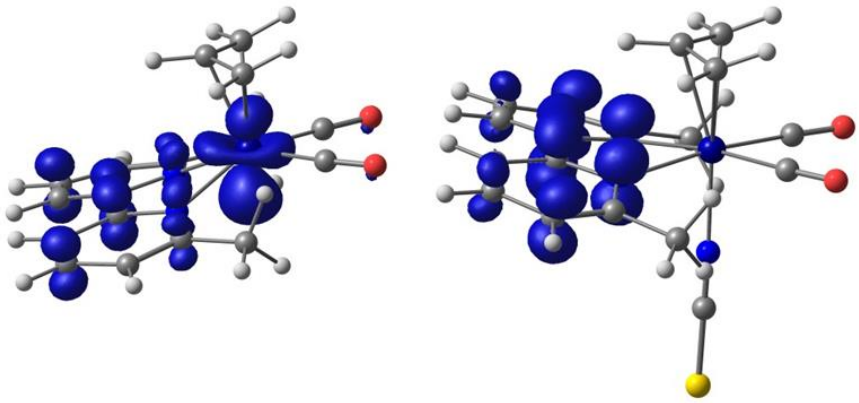

Figure DFT-S7. DFT calculated spin densities the 5-coordinate radical [Mo(η^3-allyl)$(CO)_2$(6,6′-dmbipy), [**3**-R] (the SP isomer**,** left) and radical anion [**3**]$^{\bullet-}$ (right).

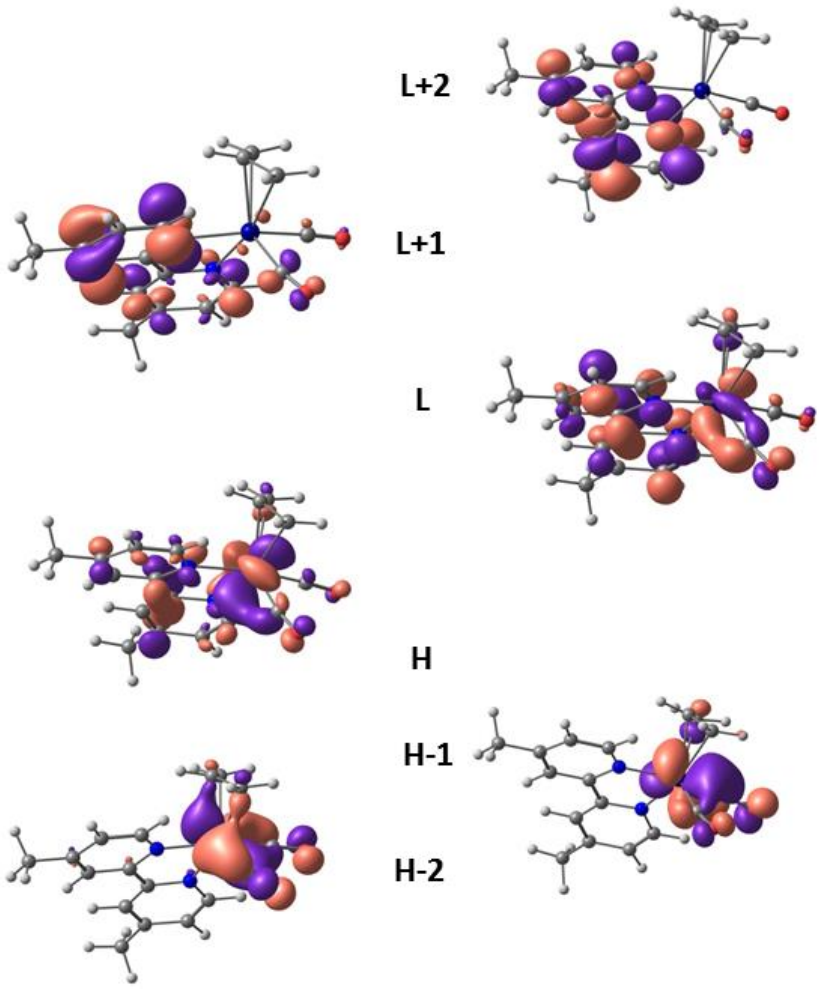

Figure DFT-S8. DFT-calculated frontier orbitals of the 5-coordinate anion [Mo(η^3-allyl)$(CO)_2$(4,4′-dmbipy)], **[1**-A]$^-$.

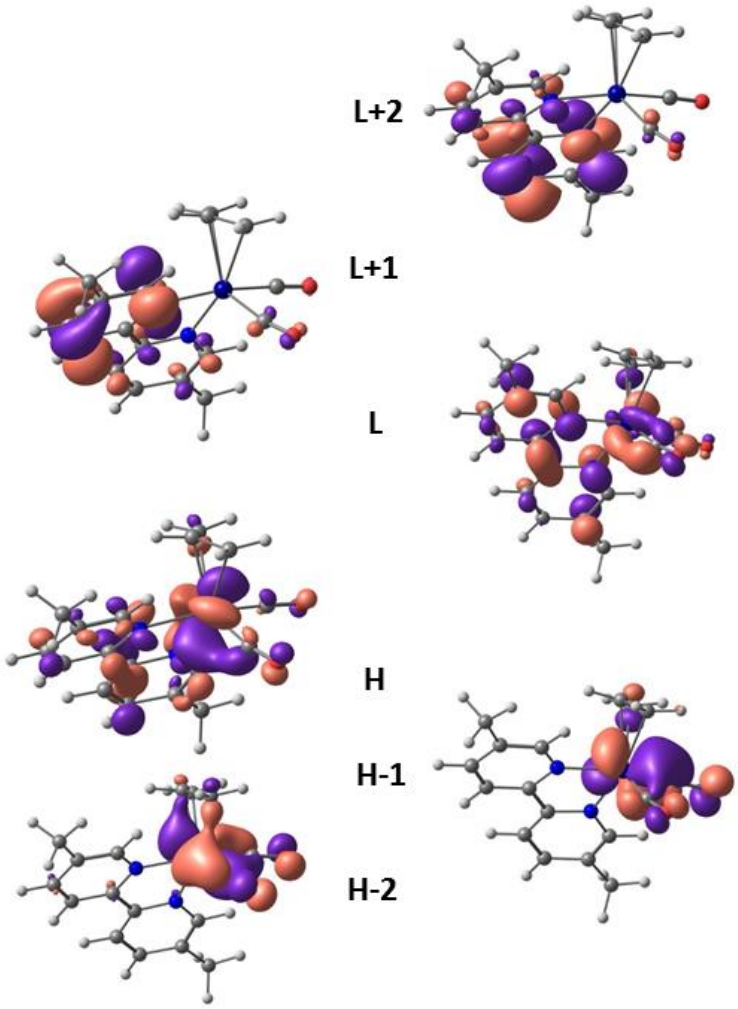

Figure DFT-S9. DFT-calculated frontier orbitals of the 5-coordinate anion [Mo(η^3-allyl)$(CO)_2$(5,5′-dmbipy)], [**2**-A]$^-$.

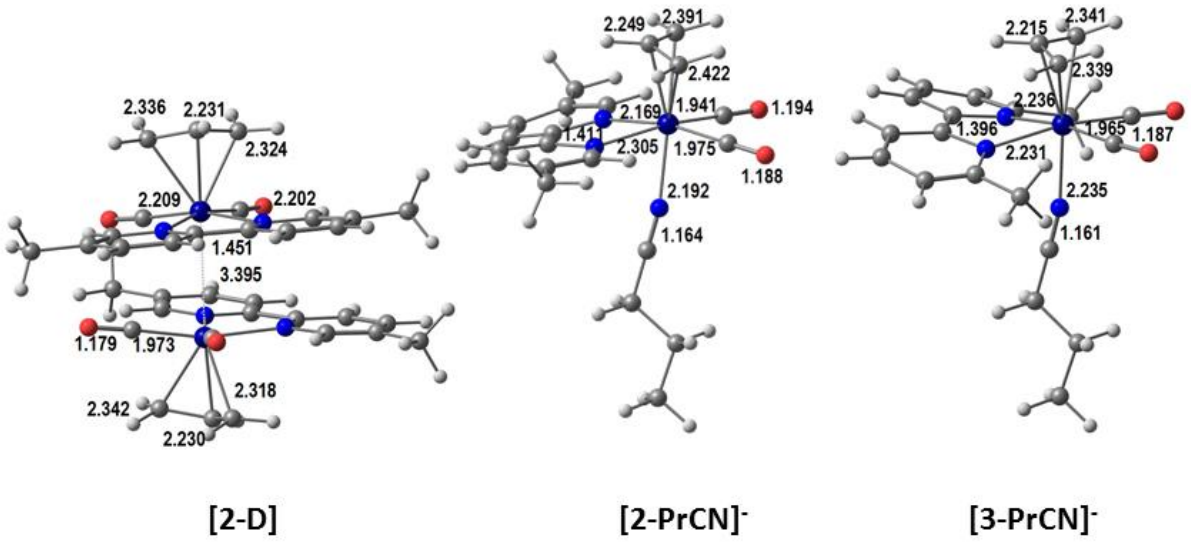

Figure DFT-S10. DFT optimized structures of the Mo–Mo dimer [Mo(η^3-allyl)(CO)$_2$(5,5′-dmbipy)]$_2$, **[2**-D] (left), the 6-coordinate anions [Mo(η^3-allyl)(CO)$_2$(5,5′-dmbipy)(PrCN)]$^-$, [**2**-PrCN]$^-$ (the equatorial isomer, center), and [Mo(η^3-allyl)(CO)$_2$(6,6′-dmbipy)(PrCN)]$^-$, [**3**-PrCN]$^-$ (the equatorial isomer, right), with relevant bond lengths (Å).

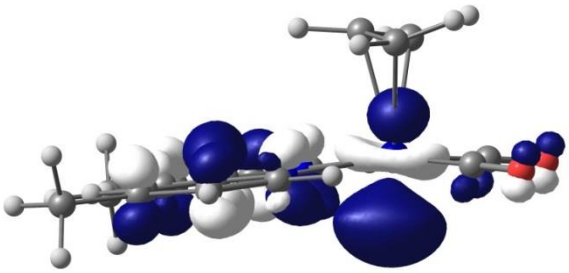

Figure DFT-S11. DFT calculated SOMO of the SP radical fragment [Mo(η^3-allyl)(CO)$_2$(4,4′-dmbipy)], [**1**-R′], used to form dimer [**1**-D].

Table E-S1. Redox potentials (V vs Fc/Fc$^+$) of complexes **1-3** and their reduction products (see Scheme 1) from cyclic voltammetry at an Au disk microelectrode at 298 K (unless stated otherwise).

Complex	Solvent	Mo(II/III) $E_{1/2}$	R1 $E_{p,c}$	R2 $E_{p,c}$	R2′ $E_{p,c}$	O1′ $E_{p,a}$	R(D) $E_{p,c}$	O(D) $E_{p,a}$
[Mo(η^3-allyl)(CO)$_2$(bipy)(NCS)][c]	THF	0.20	-1.99	-	-2.82	-1.74	-2.52	[e]
	PrCN	0.22	-1.95	-2.59	-2.77	-1.74	[e]	-0.80
	PrCN [b]	[d]	-1.88[a]	-2.58[b]	[f]	-1.58	[e]	-0.63
[Mo(η^3-allyl)(CO)$_2$(4,4′-dmbipy)(NCS)] (**1**)	THF	0.18	-2.06	-	-2.78	-1.82	-2.46	-1.18
	THF [b]	0.22	-1.96[a]	-2.53	-2.80[a]	-1.68	[e]	-1.17
	PrCN	0.22	-1.99	-	[f]	-1.74	-2.36	[e]
	PrCN [b]	0.22	-1.96[a]	-2.55	[f]	-1.54	[e]	-1.16
[Mo(η^3-allyl)(CO)$_2$(5,5′-dmbipy)(NCS)] (**2**)	THF	0.15	-2.14	-	-2.90	-1.81	-2.50	-1.18
	THF [b]	0.17	-2.07[a]	-2.60	-2.94[a]	-1.73	[e]	-1.17
	PrCN	0.22	-2.04	-	[f]	-1.73	-2.33	[e]
	PrCN [b]	0.23	-1.99[a]	-2.52	[f]	-1.62	-	[e]
[Mo(η^3-allyl)(CO)$_2$(6,6′-dmbipy)(NCS)] (**3**)	THF	0.26	-2.02[a]	-2.57	-2.94	-1.84	-	-
	THF [b]	0.28	-1.98[a]	-2.60	-2.82[a]	-1.66	-	-
	PrCN	0.32	-1.93[a]	-2.45	[f]	-1.73	-	-
	PrCN [b]	0.28	-1.94[a]	-2.56	[f]	-1.54	-	-

[a] $E_{1/2}$ value (anodic counter wave observed). [b] Measured at 195 K. [c] Measured at a Pt electrode.[45] [d] Not measured. [e] Not observable. [f] Beyond the accessible cathodic potential window of PrCN/TBAH.

Table E-S2. Redox potentials in (V vs Fc/Fc^+) of complexes **1**-**3** and their reduction products (see Scheme 1) from cyclic voltammetry at a Pt disk microelectrode at 298 K (unless stated otherwise).

Complex	Solvent	Mo(II/III) $E_{1/2}$	R1 $E_{p,c}$	R2 $E_{p,c}$	R2′ $E_{p,c}$	O1′ $E_{p,a}$	R(D) $E_{p,c}$	O(D) $E_{p,a}$
[Mo(η^3-allyl)(CO)$_2$(4,4′-dmbipy)(NCS)] **(1)**	THF	0.15	-1.79	-	-2.58	-1.48	-2.23	[c]
	THF[b]	0.18	-1.64[a]	-2.26	-2.50[a]	-1.35	[c]	[c]
	PrCN	0.20	-2.05	-	[d]	-1.77	-2.37	[c]
	PrCN[b]	0.25	-1.91[a]	-2.63	[d]	-	[c]	[c]
[Mo(η^3-allyl)(CO)$_2$(5,5′-dmbipy)(NCS)] **(2)**	THF	0.17	-1.95	-	-2.89	-1.57	-2.58	-1.13
	THF[b]	0.20	-1.94[a]	-2.54	-2.82[a]	-1.54	[c]	[c]
	PrCN	0.21	-2.05	-	[d]	-1.73	-2.61	[c]
	PrCN[b]		-1.91[a]	-2.65	[d]	-1.57	[c]	[c]
[Mo(η^3-allyl)(CO)$_2$(6,6′-dmbipy)(NCS)] **(3)**	THF	0.26	-1.88[a]	-2.56		-1.47	-	-
	THF[b]	0.34	-1.84[a]	-2.43	-2.58[a]	-1.27	-	-
	PrCN	0.31	-1.81[a]	-2.37	[d]	-1.74	-	-
	PrCN[b]	0.35	-1.79[a]	-2.46	[d]	-1.41	-	-

[a] $E_{1/2}$ value (anodic counter wave observed). [b] Measured at 195 K. [c] Not observable. [d] Beyond the accessible potential window of the electrolyte.

Table E-S3. IR and UV-vis absorption data for complexes [Mo(η^3-allyl)(CO)$_2$(*x,x′*-dmbipy)(NCS)], **1** (*x* = 4), **2** (*x* = 5) and **3** (*x* = 6), and 1e$^-$ oxidized [Mo(η^3-allyl)(CO)$_2$(*x,x′*-dmbipy)(NCS)]$^+$, [**1**]$^+$-[**3**]$^+$. Reference compounds containing the non-methylated bipyridine ligand are also included.

Complex	ν(CO)/cm^{-1}	ν(CN)/cm^{-1}	λ_{max}/ nm
[Mo(η^3-allyl)(CO)$_2$(bipy)(NCS)]^a	1950, 1866	2083	^{f}
[Mo(η^3-allyl)(CO)$_2$(bipy)(NCS)]^b	1947, 1864	2085	^{f}
[Mo(η^3-allyl)(CO)$_2$(4,4′-dmbipy)(NCS)]^c	1949, 1869	2076	490
[Mo(η^3-allyl)(CO)$_2$(4,4′-dmbipy)(NCS)]^d	1949, 1866	2080	475
[Mo(η^3-allyl)(CO)$_2$(5,5′-dmbipy)(NCS)]^c	1951, 1971	2076	480
[Mo(η^3-allyl)(CO)$_2$(5,5′-dmbipy)(NCS)]^d	1949, 1866	2080	470
[Mo(η^3-allyl)(CO)$_2$(6,6′-dmbipy)(NCS)]^c	1948, 1866	2074	460
[Mo(η^3-allyl)(CO)$_2$(6,6′-dmbipy)(NCS)]^d	1946, 1862	2078	460
[Mo(η^3-allyl)(CO)$_2$(bipy)(NCS)]$^{+a}$	2069, 2028^e	2028^e	^{f}
[Mo(η^3-allyl)(CO)$_2$(bipy)(NCS)]$^{+b}$	2069, 2019	2034	^{f}
[Mo(η^3-allyl)(CO)$_2$(4,4′-dmbipy)(NCS)]$^{+c}$	2065, 2022^e	2022^e	375, 560
[Mo(η^3-allyl)(CO)$_2$(4,4′-dmbipy)(NCS)]$^{+d}$	2067, 2024^e	2024^e	380, 550
[Mo(η^3-allyl)(CO)$_2$(5,5′-dmbipy)(NCS)]$^{+c}$	2067, 2022^e	2022^e	395, 570
[Mo(η^3-allyl)(CO)$_2$(5,5′-dmbipy)(NCS)]$^{+d}$	2068, 2024^e	2024^e	370, 543
[Mo(η^3-allyl)(CO)$_2$(6,6′-dmbipy)(NCS)]$^{+c}$	2059, 2019^e	2019^e	375, 585
[Mo(η^3-allyl)(CO)$_2$(6,6′-dmbipy)(NCS)]$^{+d}$	2059, 2019^e	2019^e	400, 553

^{a} Measured in MeCN. ^{b} Measured in PrCN at 183 K. ^{c} Measured in THF. ^{d} Measured in PrCN. ^{e} Broad band, due to strong overlap of ν_a(CO) and ν(CN) of NCS$^-$. ^{f} Not measured.

Table E-S4. IR and UV-vis absorption data for the complexes [Mo(η^3-allyl)(CO)$_2$(*x,x′*-dmbipy)(NCS)], **1** (*x* = 4), **2** (*x* = 5) and **3** (*x* = 6), and their reduction products (Scheme 1). Reference compounds containing the non-methylated bipy ligand are also included.

Complex	ν(CO)/ cm^{-1}	Calculated[h] ν(CO)/ cm^{-1}	ν(CN)/ cm^{-1}	Calculated[h] ν(CN)/ cm^{-1}	λ_{max}/ nm
[Mo(η^3-allyl)((CO)$_2$(bipy)(NCS)] [a]	1950, 1868	-	2079	-	351, 478
[Mo(η^3-allyl)(CO)$_2$(bipy)(NCS)] [a,c]	1946, 1864	-	2085	-	-
[Mo(η^3-allyl)(CO)$_2$(bipy)(NCS)] [b]	1951, 1871	-	2075	-	340, 501
[Mo(η^3-allyl)(CO)$_2$(4,4′-dmbipy)(NCS)] [a]	1949, 1866	-	2080	-	475
[Mo(η^3-allyl)(CO)$_2$(4,4′-dmbipy)(NCS)] [a,c]	1946, 1863	-	2084	-	-
[Mo(η^3-allyl)(CO)$_2$(4,4′-dmbipy)(NCS)] [b]	1949, 1869	1882, 1800	2076	2056	490
[Mo(η^3-allyl)(CO)$_2$(4,4′-dmbipy)(NCS)] [b,d]	1948, 1868	-	2078	-	-
[Mo(η^3-allyl)(CO)$_2$(5,5′-dmbipy)(NCS)] [a]	1950, 1867	-	2080	-	470
[Mo(η^3-allyl)(CO)$_2$(5,5′-dmbipy)(NCS)] [a,c]	1947, 1863	-	2085	-	-
[Mo(η^3-allyl)(CO)$_2$(5,5′-dmbipy)(NCS)] [b]	1951, 1871	1883, 1801	2076	2056	-
[Mo(η^3-allyl)(CO)$_2$(6,6′-dmbipy)(NCS)] [a]	1946, 1862	-	2078	-	460
[Mo(η^3-allyl)(CO)$_2$(6,6′-dmbipy)(NCS)] [a,c]	1944, 1860	-	2082	-	-
[Mo(η^3-allyl)(CO)$_2$(6,6′-dmbipy)(NCS)] [b]	1948, 1866	1881, 1800	2074	2054	-
[Mo(η^3-allyl)(CO)$_2$(bipy)(NCS)]$^{\bullet-}$ [a,c]	1920, 1829	-	2092	-	-
[Mo(η^3-allyl)(CO)$_2$(4,4′-dmbipy)(NCS)]$^{\bullet-}$ [a,c]	1922, 1832	1855, 1763	2089	2070	388, 494, 538, > 600
[Mo(η^3-allyl)(CO)$_2$(4,4′-dmbipy)(NCS)]$^{\bullet-}$ [b,d]	1926, 1831		2084		
[Mo(η^3-allyl)(CO)$_2$(5,5′-dmbipy)(NCS)]$^{\bullet-}$ [a,c]	1921, 1832	1853, 1761	2085	2072	394, 492, 528, > 600
[Mo(η^3-allyl)(CO)$_2$(6,6′-dmbipy)(NCS)]$^{\bullet-}$ [a,c]	1920, 1829	1855, 1764	2089	2069	396, 489, 518, > 600
[Mo(η^3-allyl)(CO)$_2$(6,6′-dmbipy)(NCS)]$^{\bullet-}$ [b]	1925, 1834	-	2089	-	-
[Mo(η^3-allyl)(CO)$_2$(6,6′-dmbipy)(NCS)]$^{\bullet}$ [a]	1923, 1833	-		-	-
[Mo(η^3-allyl)(CO)$_2$(bipy)(PrCN)]$^-$ [a]	1893, 1796	-	2147[i]	-	-
[Mo(η^3-allyl)(CO)$_2$(4,4′-dmbipy)(PrCN)]$^-$ [a,c]	1896, 1797	1797, 1705	2148[i]	2229	350
[Mo(η^3-allyl)(CO)$_2$(5,5′-dmbipy)(PrCN)]$^-$ [a,c]	1897, 1789	1781, 1687	2148[i]	2213	360
[Mo(η^3-allyl)(CO)$_2$(6,6′-dmbipy)(PrCN)]$^-$ [a]	1904, 1789	1816, 1715	2148[i]	2247	-
[Mo(η^3-allyl)(CO)$_2$(bipy)]$_2$ [b]	1891,1778, 1757	-	-	-	369, 581
[Mo(η^3-allyl)(CO)$_2$(4,4′-dmbipy)]$_2$ [b]	1891,1776, 1759	1775,1787, 1844,1858	-	-	-
[Mo(η^3-allyl)(CO)$_2$(5,5′-dmbipy)]$_2$ [b]	1892,1779, 1757	1777,1789, 1844,1858	-	-	-
[Mo(η^3-allyl)(CO)$_2$(4,4′-dmbipy)]$^-$ [b,d]	1815, 1722	1741, 1656[e]		-	
[Mo(η^3-allyl)(CO)$_2$(5,5′-dmbipy)]$^-$ [a,c]	1789, 1693	1742, 1658[e]	-	-	590
[Mo(η^3-allyl)(CO)$_2$(5,5′-dmbipy)]$^-$ [b]	1820, 1730	-		-	
[Mo(η^3-allyl)(CO)$_2$(6,6′-dmbipy)]$^-$ [a,c]	1797, 1700[g]	1803, 1702[f]	-	-	420, 550
[Mo(η^3-allyl)(CO)$_2$(6,6′-dmbipy)]$^-$ [a]	1807, 1700	-	-	-	-
[Mo(η^3-allyl)(CO)$_2$(6,6′-dmbipy)]$^-$ [b]	1792, 1680 [j]	-	-	-	-

[a] Measured in PrCN, [b] Measured in THF. [c] Measured at 223 K. [d] Measured at 268 K. [e] Calculated axial isomer. [f] Calculated equatorial isomer. [g] Broad absorption bands. [h] Some DFT-calculated data from Table DFT-S5 are reproduced here for clarity. [i] CN stretching mode of the PrCN ligand. [j] Values at an Au minigrid working electrode; the ν(CO) values at a Pt minigrid are 1801 and 1717 cm^{-1}.

Cyclic voltammetry of complexes 1-3 in PrCN at an Au disk microelectrode

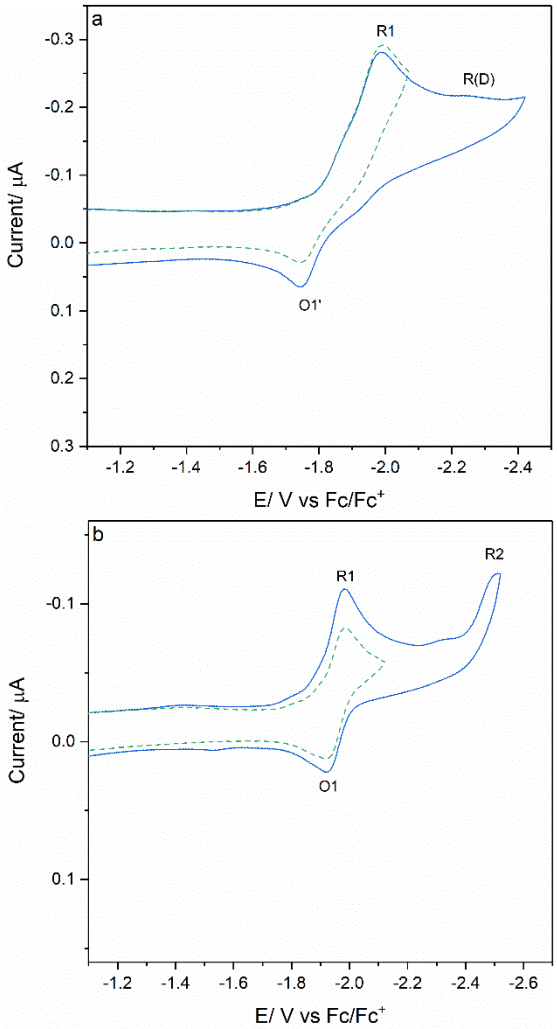

Figure E-S1. Cyclic voltammetry of [Mo(η^3-allyl)$(CO)_2$(4,4′-dmbipy)(NCS)] (**1**) at (a) room temperature and (b) 195 K in PrCN/TBAH. Au disk microelectrode. Scan rate: 100 mV s^{-1}.

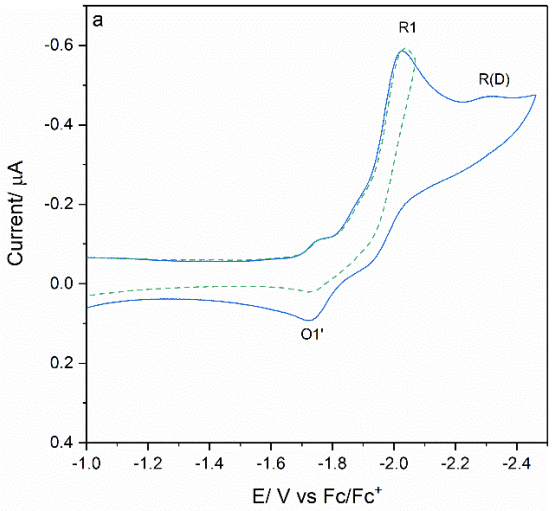

Figure E-S2. Cyclic voltammetry of [Mo(η^3-allyl)(CO)$_2$(5,5′-dmbipy)(NCS)] (**2**) at room temperature in PrCN/TBAH. Au disk microelectrode. Scan rate: 100 mV s^{-1}.

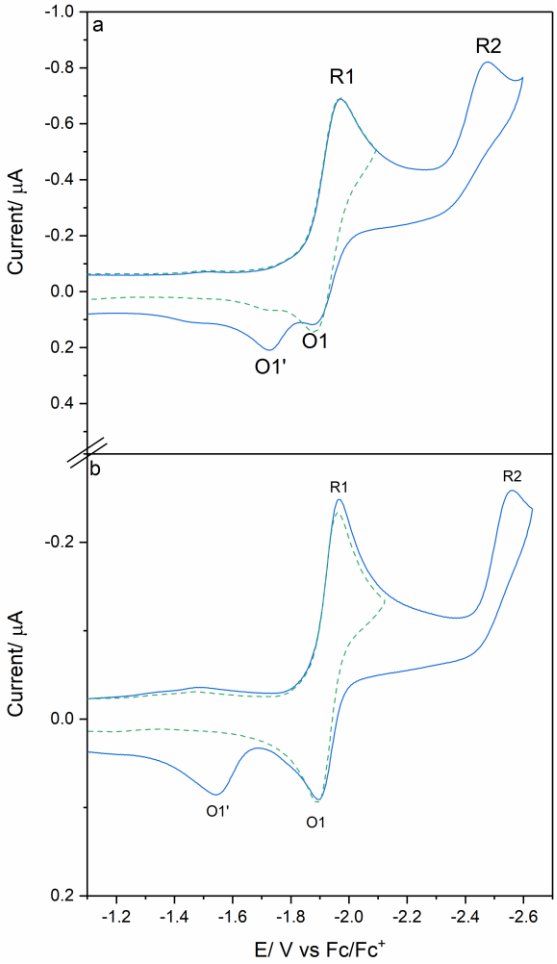

Figure E-S3. Cyclic voltammetry of [Mo(η^3-allyl)(CO)$_2$(6,6′-dmbipy)(NCS)] (**3**) at (a) room temperature and (b) 195 K in PrCN/TBAH. Au microdisc electrode. Scan rate: 100 mV s^{-1}.

Cyclic voltammetry of complexes 1-3 in THF at a Pt microdisc eleclectrode

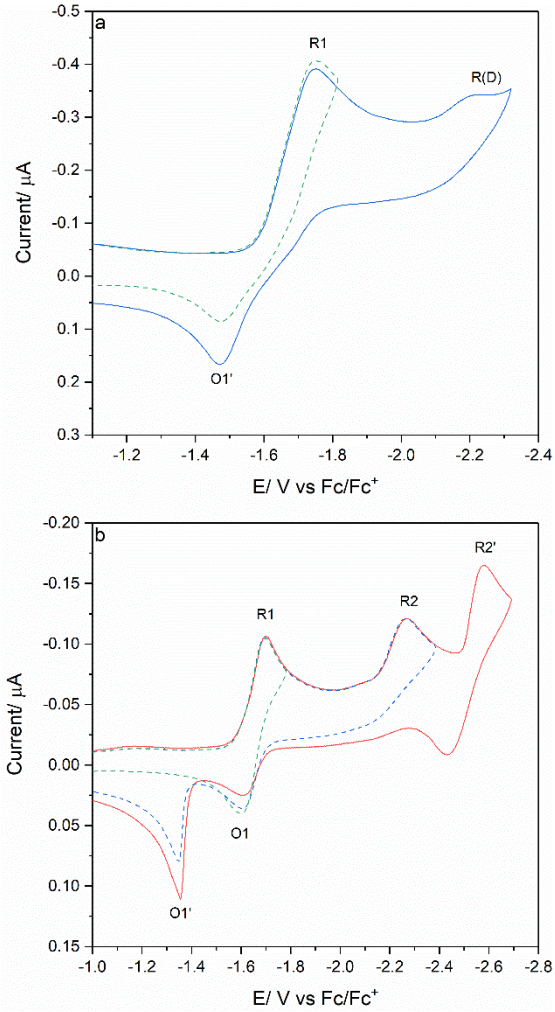

Figure E-S4. Cyclic voltammetry of [Mo(η^3-allyl)$(CO)_2$(4,4′-dmbipy)(NCS)] (**1**) at (a) room temperature and (b) low temperature (195 K) in THF/TBAH. Pt disk microelectrode. Scan rate: 100 mV s^{-1}.

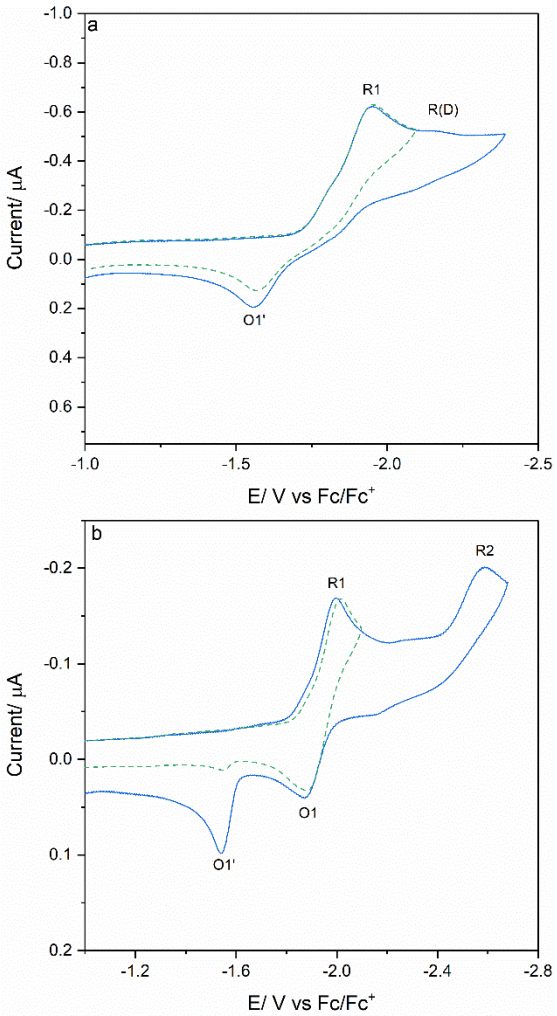

Figure E-S5. Cyclic voltammetry of [Mo(η^3-allyl)$(CO)_2$(5,5′-dmbipy)(NCS)] (**2**) at (a) room temperature and (b) 195 K in THF/TBAH. Pt disk microelectrode. Scan rate: 100 mV s^{-1}.

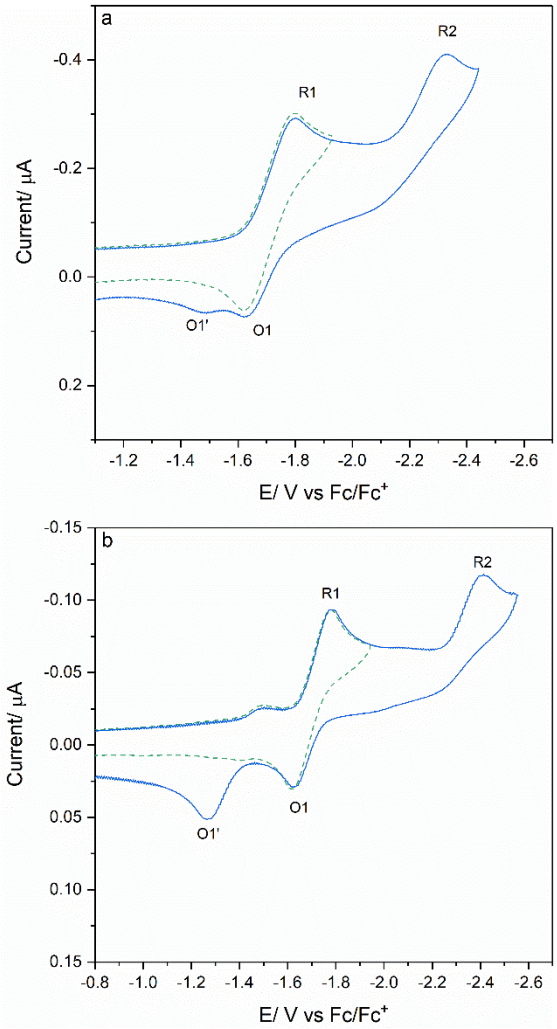

Figure E-S6. Cyclic voltammetry of [Mo(η^3-allyl)$(CO)_2$(6,6′-dmbipy)(NCS)] (**3**) at (a) room temperature and (b) 195 K in THF/TBAH. Pt disk microelectrode. Scan rate: 100 mV s^{-1}.

Cyclic voltammetry of complexes 1-3 in PrCN at a Pt disk microelectrode

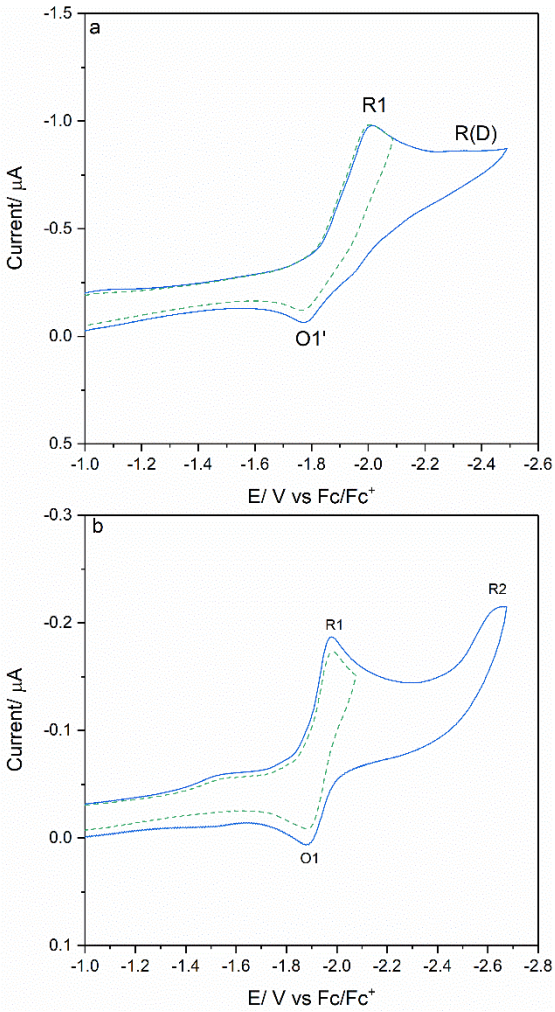

Figure E-S7. Cyclic voltammetry of [Mo(η^3-allyl)(CO)$_2$(4,4′-dmbipy)(NCS)] (**1**) at (a) room temperature and (b) 195 K in PrCN/TBAH. Pt disk microelectrode. Scan rate: 100 mV s^{-1}.

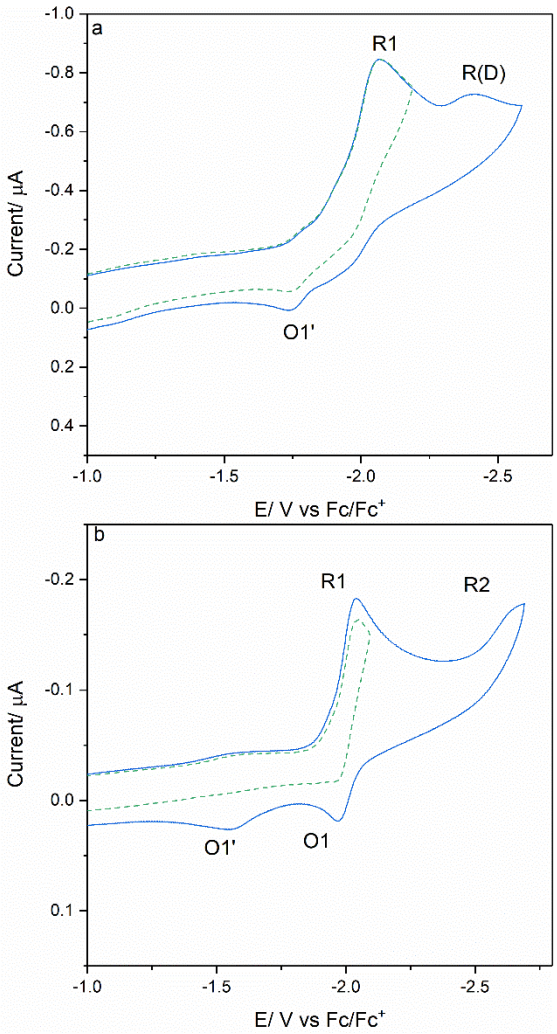

Figure E-S8. Cyclic voltammetry of [Mo(η^3-allyl)$(CO)_2$(5,5′-dmbipy)(NCS)] (**2**) at (a) room temperature and (b) 195 K in PrCN/TBAH. Pt disk microelectrode. Scan rate: 100 mV s^{-1}.

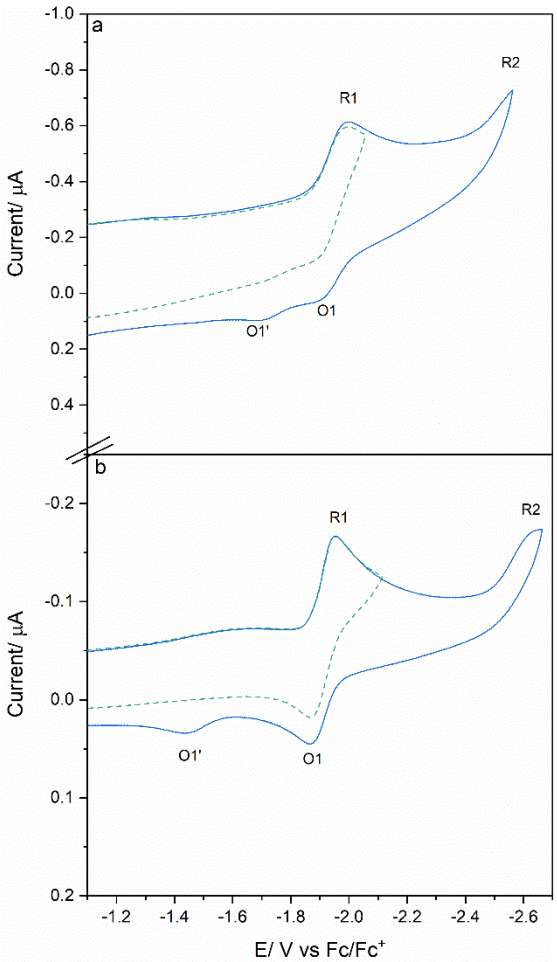

Figure E-S9. Cyclic voltammetry of [Mo(η^3-allyl)$(CO)_2$(6,6′-dmbipy)(NCS)] (**3**) at (a) room temperature and (b) 195 K in PrCN/TBAH. Pt disk microelectrode. Scan rate: 100 mV s^{-1}.

Cathodic IR and UV-vis spectroelectrochemistry of complexes 1-3 in PrCN at 223 K

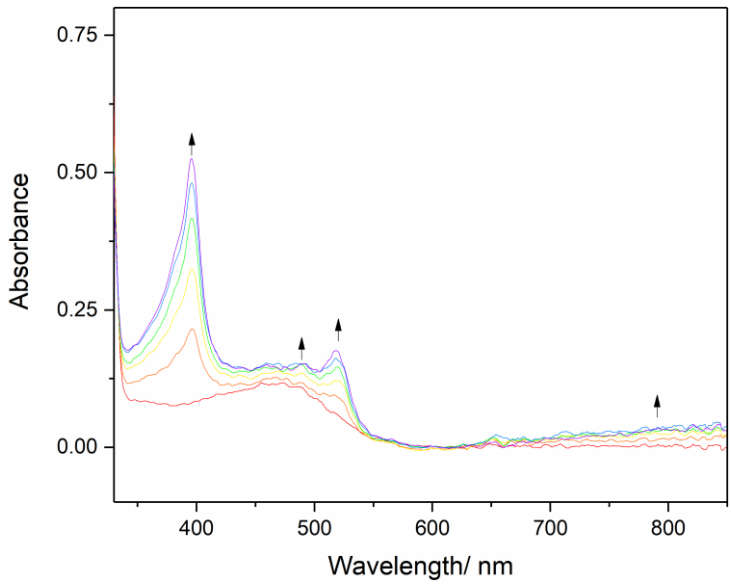

Figure E-S10. Cathodic UV-vis spectroelectrochemistry of [Mo(η^3-allyl)(CO)$_2$(6,6′-dmbipy)(NCS)] (**3**) in PrCN/TBAH at 223 K, showing its conversion to stable radical anion [**3**]$^{\bullet-}$ (↑) at the cathodic wave R1, using a cryostated OTTLE cell.

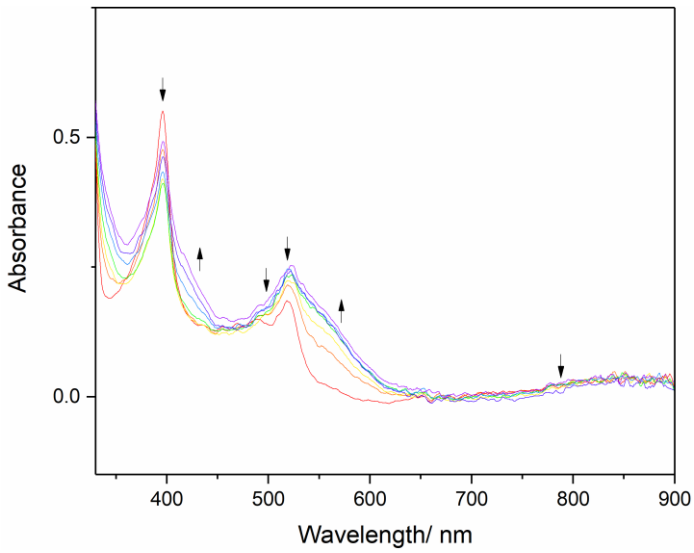

Figure E-S11. Cathodic UV-vis spectroelectrochemistry of [Mo(η^3-allyl)(CO)$_2$(6,6′-dmbipy)(NCS)] (**3**) in PrCN/TBAH at 223 K, showing the conversion of [**3**]$^{\bullet-}$ (↓) to 5-coordinate anion [**3**-A]$^-$ (↑) at the cathodic wave R2. The electrolysis was conducted in a cryostated OTTLE cell.

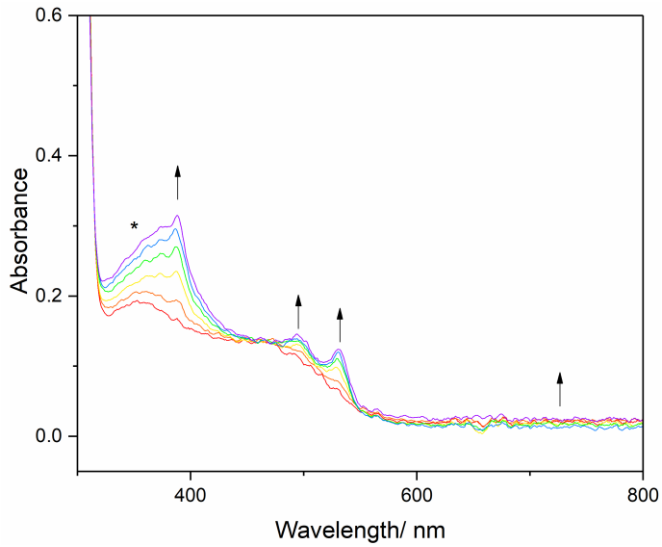

Figure E-S12. UV-vis spectral changes recorded during the electrochemical reduction of [Mo(η^3-allyl)$(CO)_2$(4,4′-dmbipy)(NCS)] (**1**) at 223 K in PrCN/TBAH within a cryostated OTTLE cell. In line with Figure 13 (in the main text), the spectra reveal the formation of radical anion [**1**]$^{\bullet-}$ (↑), showing the characteristic bifurcated π*π* intra-ligand absorption of [dmbipy]$^{\bullet-}$ around 500 nm, and 6-coordinate anion [**1**-PrCN]$^-$ (*) (Scheme 1).

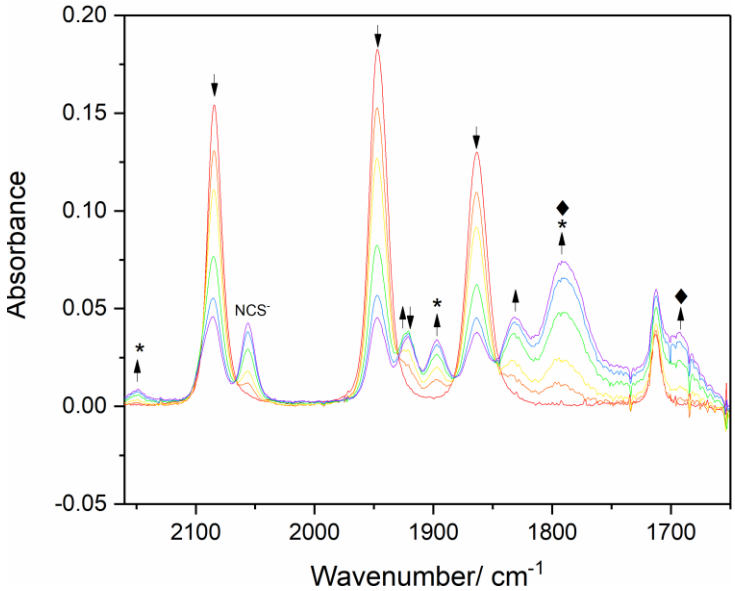

Figure E-S13. IR SEC monitoring of the reduction of [Mo(η^3-allyl)$(CO)_2$(5,5′-dmbipy)(NCS)] (**2**) (↓) in PrCN/TBAH at 223 K, producing radical anion [**2**]$^{\bullet-}$ (↑↓), and 2e$^-$ reduced 6-coordinate [**2**-PrCN]$^-$ (*) co-existing in an equilibrium with 2e$^-$ reduced 5-coordinate [**2**-A]$^-$ (♦).

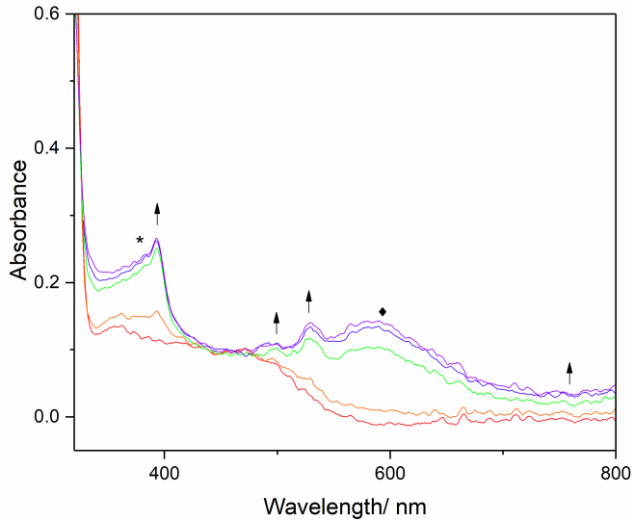

Figure E-S14. UV-vis spectroelectrochemistry of [Mo(η^3-allyl)$(CO)_2$(5,5′-dmbipy)(NCS)] (**2**), red line, in PrCN/TBAH at 223 K, showing its reduction to intermediate [**2**]$^{\bullet-}$ (↑) that transforms concomitantly to two 2e$^-$ reduced species in an equilibrium, viz. 6-coordinate [**2**-PrCN]$^-$ (*) and 5-coordinate [**2**-A]$^-$ (♦). The electrolysis was conducted in a cryostated OTTLE cell.

Cathodic IR spectroelectrochemistry of complexes 1-3 in THF or PrCN at room temperature

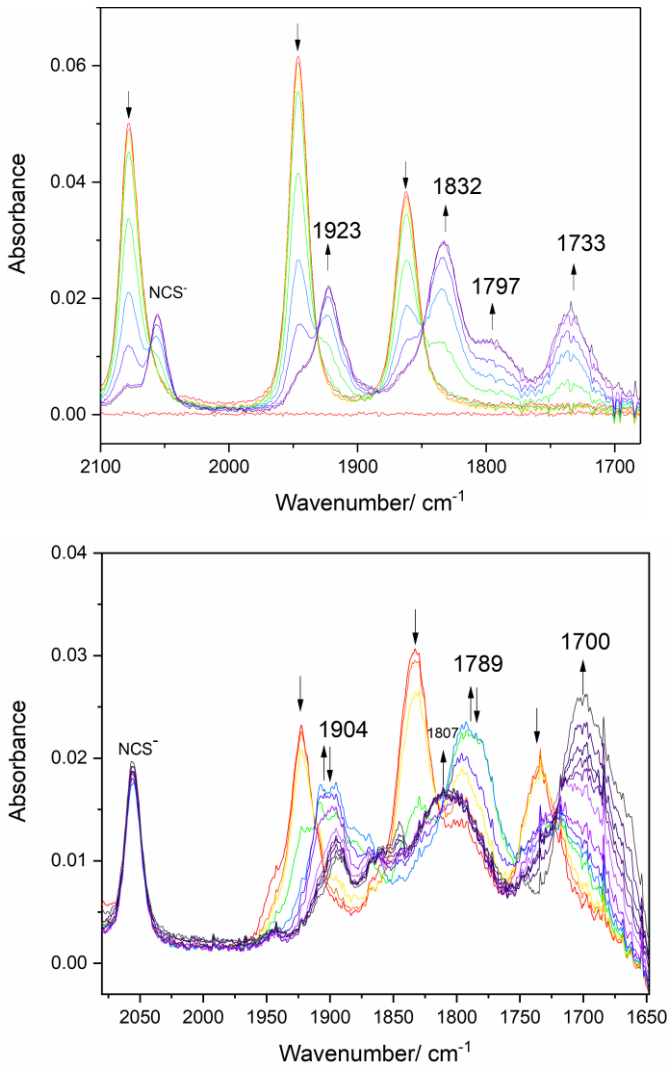

Figure E-S15. IR spectroelectrochemistry of complex [Mo(η^3-allyl)(CO)$_2$(6,6′-dmbipy)(NCS)] (**3**) (↓) in PrCN/TBAH at 293 K, showing (top) the reduction at R1 to give radical [**3**-PrCN] as a contact species with 2e$^-$ reduced 5-coordinate [**3**-A]$^-$, and (bottom) the concomitant cathodic step converting [**3**-PrCN] (↓) to [**3**-PrCN]$^-$ (↑↓) that further transforms to [**3**-A]$^-$ (↑).

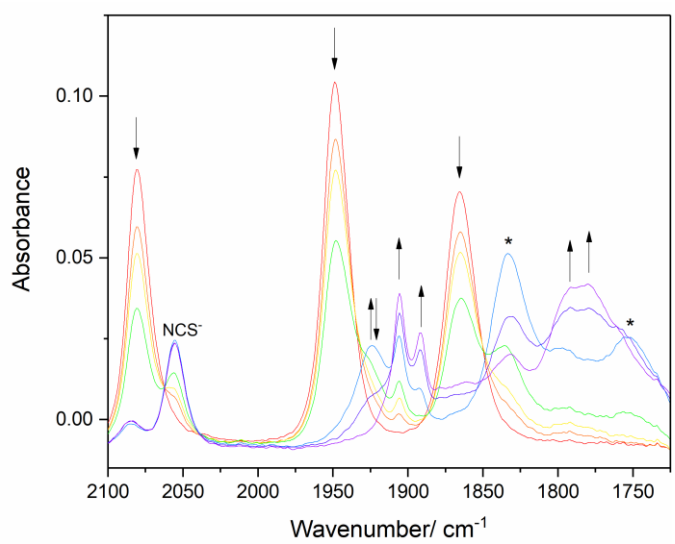

Figure E-S16. IR SEC monitoring of the reduction of [Mo(η^3-allyl)(CO)$_2$(4,4′-dmbipy)(NCS)] (**1**) (↓) in PrCN/TBAH at 293 K to radical [**1**-PrCN] (↓↑) and 2e$^-$ reduced [**1**-A]$^-$ (*) as a weak adduct with PrCN, converting ultimately to [Mo(η^3-allyl)(CO)$_2$(4,4′-dmbipy)]$_2$-related dimer [**1**-D′] (↑).

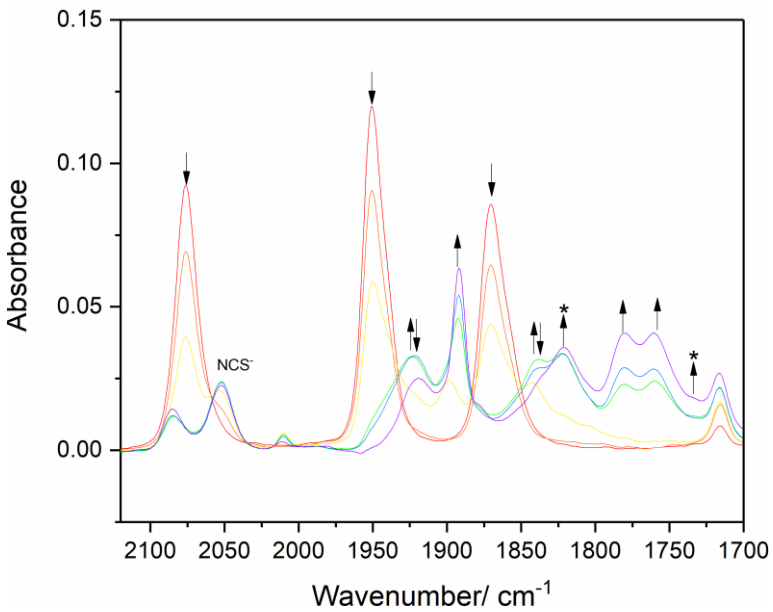

Figure E-S17. IR SEC monitoring of the initial reduction of [Mo(η^3-allyl)(CO)$_2$(5,5′-dmbipy)(NCS)] (**2**) (↓) at R1 in THF/TBAH at 293 K to intermediate [**2**]$^{\bullet-}$ (↓↑), further converting to both 2e$^-$ reduced [**2**-A]$^-$ (*) and dominant [Mo(η^3-allyl)(CO)$_2$(5,5′-dmbipy)]$_2$-related dimer [**2**-D′] (↑).

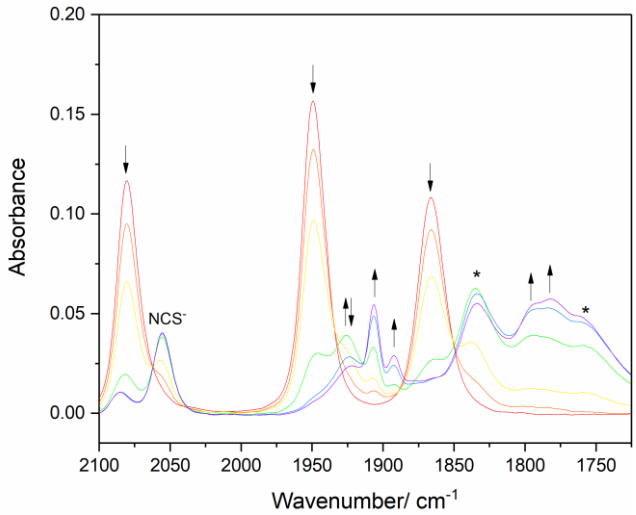

Figure E-S18. IR SEC monitoring of the reduction of [Mo(η^3-allyl)$(CO)_2$(5,5′-dmbipy)(NCS)] (**2**) (↓) in PrCN/TBAH at 293 K to radical [**2**-PrCN] (↓↑) and $2e^-$ reduced [**2**-A]$^-$ (*) as a weak adduct with PrCN, in a mixture with [Mo(η^3-allyl)$(CO)_2$(5,5′-dmbipy)]$_2$-related dimer [**2**-D′] (↑).

Cathodic IR spectroelectrochemistry of complexes 1 and 3 in CO_2 saturated THF at room temperature

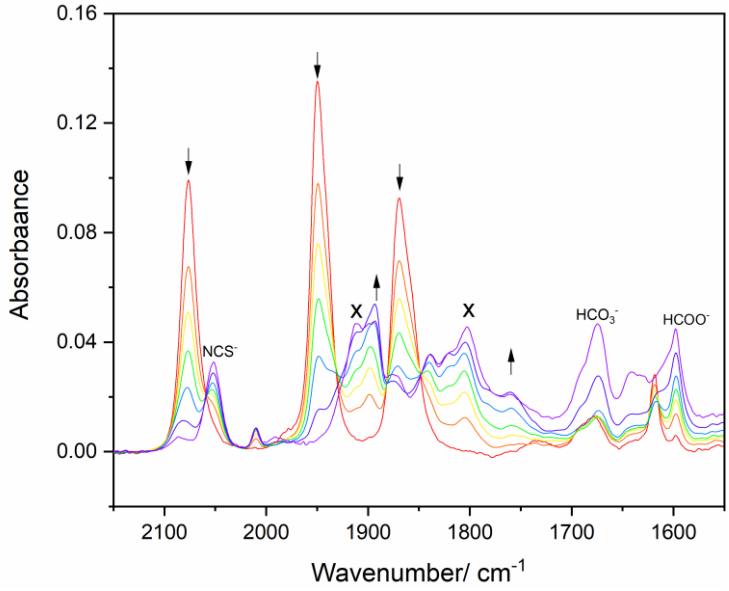

Figure E-S19. IR spectroelectrochemistry of [Mo(η^3-allyl)(CO)$_2$(4,4′-dmbipy)(NCS)] (**1**) in CO_2-saturated THF/TBAH, showing the conversion of the parent complex at R1 to [**1**-CO_2]$^-$ (×), and inactive dimer [**1**-D′] (↑).

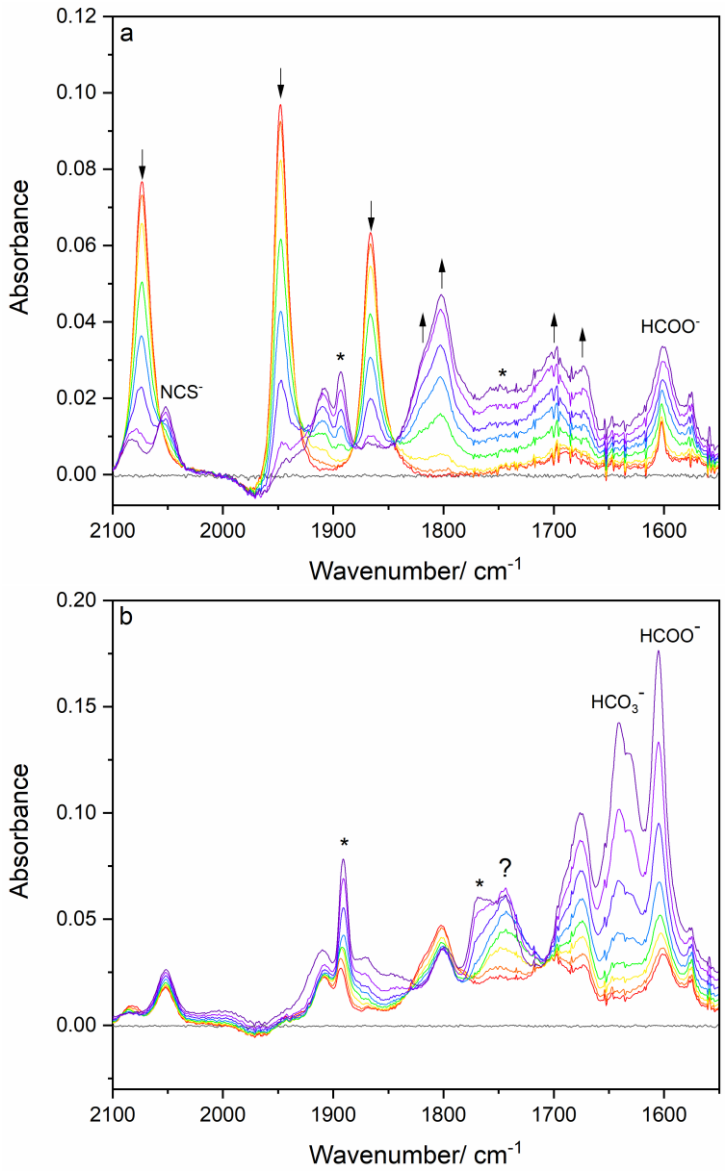

Figure E-S20. IR spectroelectrochemistry of [Mo(η^3-allyl)(CO)$_2$(4,4′-dmbipy)(NCS)] (**3**) in CO_2-saturated THF/TBAH showing (a) the conversion of the parent complex at R1 to [**3**-A]$^-$ weakly interacting with CO_2 (↑), and (b) IR spectral changes accompanying further cathodic potential shift toward the cathodic wave R2.